

# MARS EXPRESS: MOMENTUM LOADING DUE TO DISTURBANCE TORQUES AND OFF-LOADING STRATEGIES DURING THE OPERATIONAL PHASE

**Pablo PEREZ-ILLANA**

GMV, S.A.

c/ Isaac Newton 11 PTM - Tres Cantos

E-28760 Madrid - SPAIN

pppi@gmv.es    <http://www.gmv.es>

Contractor at ESA / European Space Operations Centre

Robert Bosch Str.5, D-64293 Darmstadt - GERMANY.

Pablo.Perez-Illana@esa.int    <http://www.esoc.esa.de>

**ABSTRACT** - *The loading of Mars Express angular momentum by disturbance torques is modelled in the operational orbit around Mars. Additional analytical approaches are developed e.g. for the gravity gradient contribution. The results are analysed at two maximum altitudes of observation. For the off-loading of the reaction wheels this paper presents combinations of attitude manoeuvres and thrusters actuation such that comply with solar incidence constraints and minimise fuel consumption and residual forces. The actual applicability of these strategies is to be considered along with other system constraints.*

**KEYWORDS:** Attitude, loading, angular momentum, torque, off-loading, desaturation, reaction wheels, thrusters, reaction control system, residual force.

## 1. INTRODUCTION

During the routine operations phase Mars Express orbits around Mars and the angular momentum of the spacecraft is increased by disturbance torques. The reaction wheels cannot absorb all this loading infinitely. For their desaturation, activation of the thrusters of the reaction control system is required from time to time.

The present paper deals with the computation of the angular momentum loading due to disturbance torques and different strategies of off-loading are presented in order to comply with the operational constraints and to minimise fuel consumption and residual forces.

After an overview of MEX mission in section 2., section 3. introduces the current S/C configuration and the geometrical and mass properties relevant for attitude studies. The influence of the deployment of MARSIS dipole antenna is covered as well as the offset between the solar array axis and the center of mass. The reaction wheels layout and the selected configuration of thrusters are also presented in this section.

The operational orbit is described in section 4. The operational attitude is defined in section 5. An analytical approach is developed to fix the solar array orientation during the observation period (Appendix I). The spacecraft rates are also derived (Appendix III)

The disturbance torques are evaluated in section 6. Models for the computation of the gravity gradient torque and the solar pressure torque are analysed and results for the first orbits after Mars orbit injection are shown. An estimation of order of magnitude allows to discard the effect of the aerodynamic torque on the angular momentum.

The shift of the angular momentum is given by the time integral over all the torques along inertial axes. (An analytical approach for the contribution of the gravity gradient is annexed in Appendix II). The corresponding results are shown in section 7. In this section several possibilities of off-loading are analysed, bearing in mind the various thrusters/manoeuvres combinations: e.g. off-loading directly from the initial attitude, certain S/C pre-orientation rotations followed by the activation of just one thruster (the most efficient option). Application is done for a first off-loading slot as a mere example. The treatment of the activation of two thrusters is also addressed.

Finally, the conclusions of this study are summarised in section 8.

*It should be emphasized that the analysis contained in this technical note is preliminary only, aimed at identifying possible off-loading strategies. In particular, geometrical and mass data are not definitive.*

However, overall conclusions are expected to be representative and also of interest for off-loading during other phases, such as cruise. Moreover, by similar reasoning orbit maintenance manoeuvres could be used for wheel off-loading: the residual torques at certain attitudes may contribute to desaturate the reaction wheels.

## 2. MISSION OVERVIEW

Mars Express is planned to be the first 'flexible mission' in the revised ESA Long-Term Scientific Programme and is based on a fast implementation driving to launch in June 2003. ESOC will conduct the operations using the ESA ground station in Perth. After an interplanetary cruise of 7 months the satellite will be injected in a martian orbit. The objective of the mission is the remote observation of Mars by means of seven payload instruments. The planet atmosphere, surface and subsurface will be studied via coordinated measurements.

The mission has been conceived as an orbiter observing the martian surface from a quasi-polar orbit with a pericentre altitude of about 270 km, an apocentre altitude of about 11500 km, an inclination of 86.4 deg and a period of 7.6 hours. In addition, the possibility for a lander weighting a maximum of 60 kg is retained. The orbiter would have to act as data relay for the lander. Visibility with Perth station is 8 h per day (TBC).

For each orbit, operations are split in two phases:

- Mars nadir-pointed observation phase around pericentre in which instruments data are collected and
- Earth-pointed communication phase during which data are down-linked at high rate.

One opposition period starting about day 24 after Mars insertion interrupts communications with the Earth for 30 days, during which science operations are reduced. There is no solar eclipse until 41 days after MOI. An Earth conjunction around day 667 after Mars insertion affects the command link for about 8 days.

During the extended operations phase, communications with US landers and rovers may take place. For this, the orbit apocentre may be lowered using aerobraking.

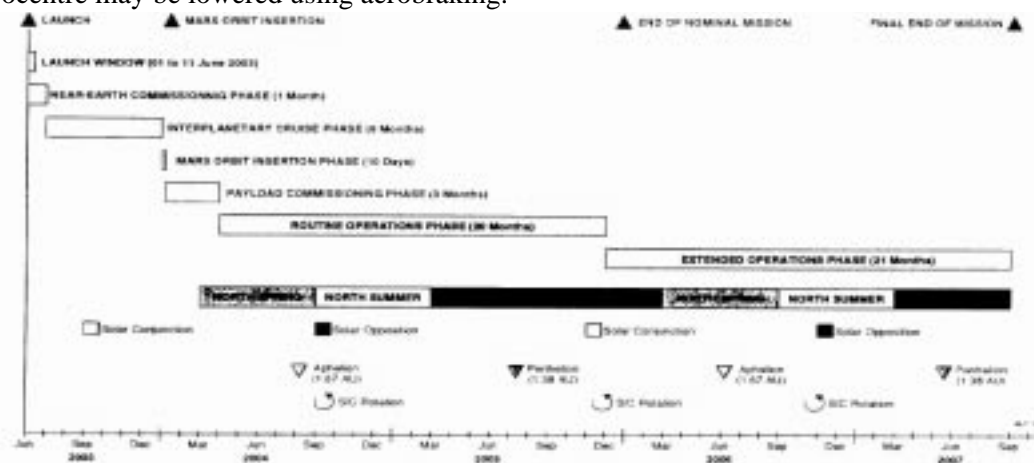
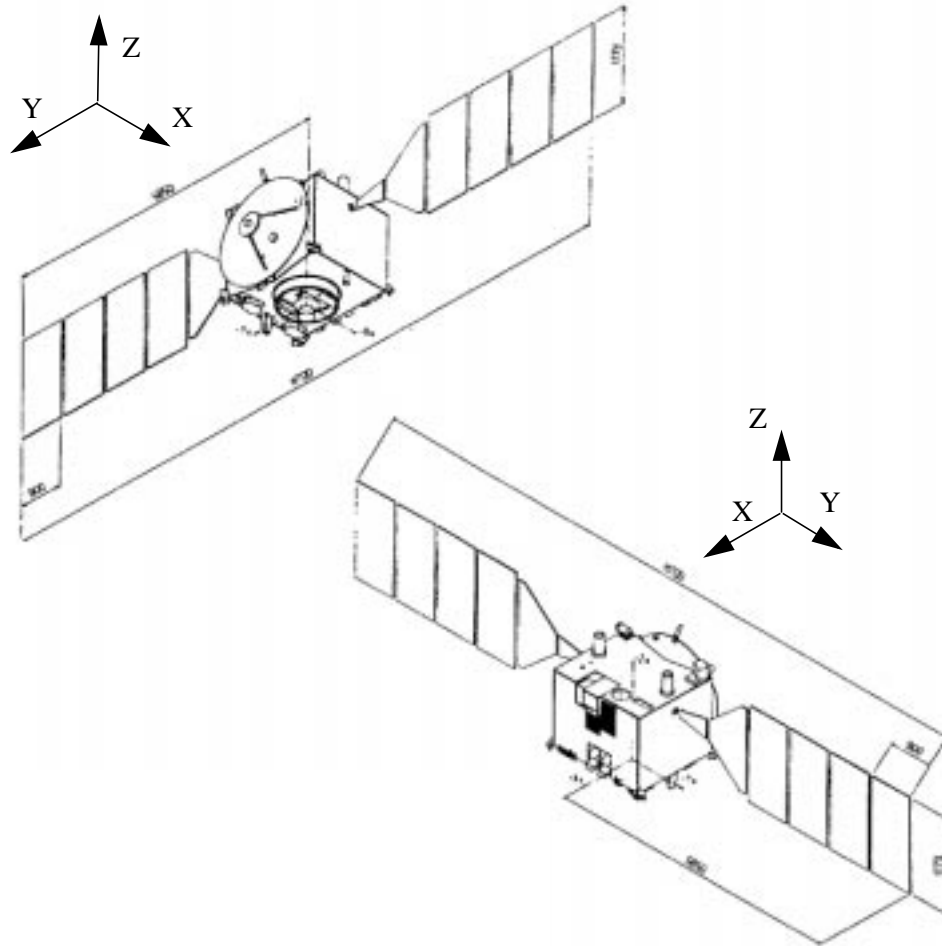


Fig. 1. Mission phases

### 3. SPACECRAFT CONFIGURATION AND DYNAMICAL MODEL

The Mars Express spacecraft design is based on a central body with fixed High Gain Antenna (HGA) and 1 degree of freedom steerable Solar Arrays. The central body is box-shaped, measuring about 1.7 m x 1.7 m x 1.4 m (see fig.2). The Solar array is composed of two wings providing a symmetrical configuration. Figure 2 shows an overview of the S/C and S/C mechanical orthogonal axes. Earth communication antenna is assumed to be mounted in direction -X axis (i.e. no HGA off-pointing wrt -X axis is considered in this note). Radiators are located on +X side. The solar array axis contains the Y-axis.



**Fig. 2. Mars Express S/C Overview**

A bi-propellant propulsion system containing a 400 N main engine along -Z axis and 10 N thrusters is used for orbit and attitude manoeuvres.

The orbiter will embark four optical nadir pointing instruments: HSRC, OMEGA, PFS and SPICAM. Viewing direction shall be the S/C Z axis.

The lander would be also mounted on the +Z face of the S/C such that effects on the X/Y components of the global CoM are minimised.

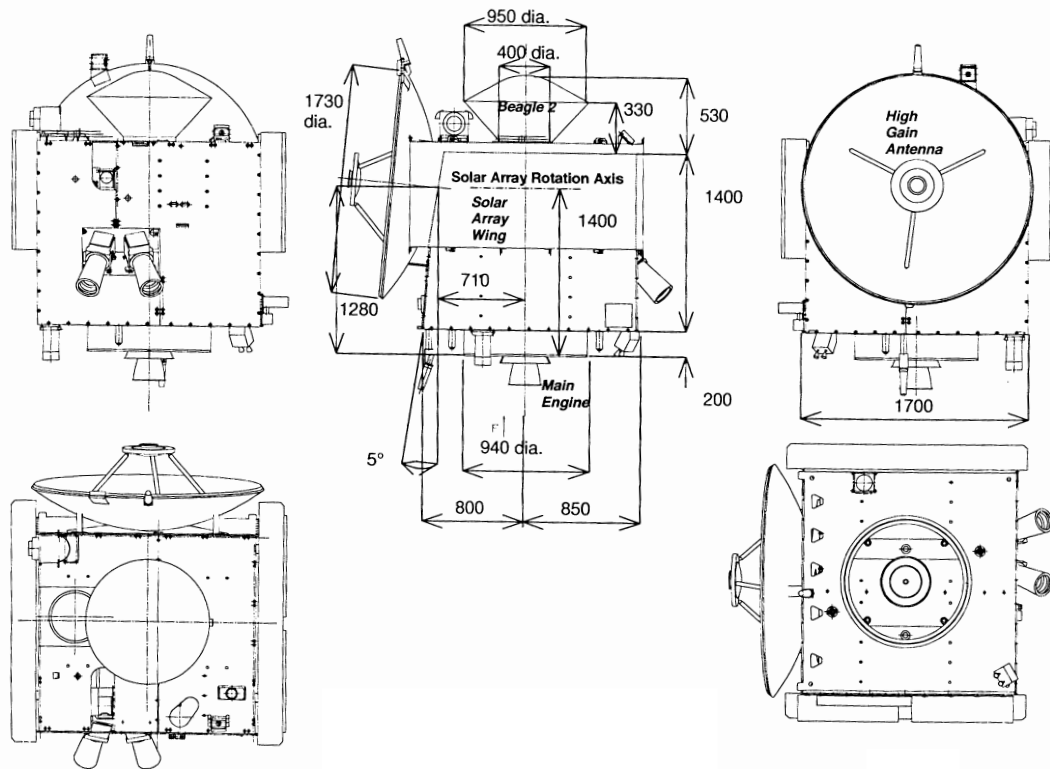


**Fig. 3. Mars Express Spacecraft**

There are two SADM, one for each wing of the SA. They are mounted on the  $\pm Y$  panels of the S/C and are controlled independently by the AOCS processor module. SADM rotation is limited to  $\pm 180$  deg by a stop mechanism. Note that the solar array axis intersects the Z-axis considerably above the position of the CoM (fig.3 and table1) in order to guarantee aerodynamic longitudinal static stability during aerobraking. This offset results in significant lever arm for the action of solar pressure, as shown in section 6.

During the operations phase (after Mars Orbit Insertion), the MARSIS dipole antenna shall be deployed along the  $\pm X$ -axis of the spacecraft (fig.4). The configuration used in this note assumes a length of 25 m for each dipole and a total MARSIS inertia of  $900 \text{ kg.m}^2$  (the initial concept was  $300 \text{ kg.m}^2$ ; a value of  $550 \text{ kg.m}^2$  would correspond to the option of  $2 \times 20 \text{ m}$ ). In any case the contribution of MARSIS to the MEX inertia tensor is therefore fundamental and it has direct influence on the gravity gradient torque. Note for instance that with MARSIS deployed the Y-axis is not the minimum inertia axis of the S/C (see table 1).

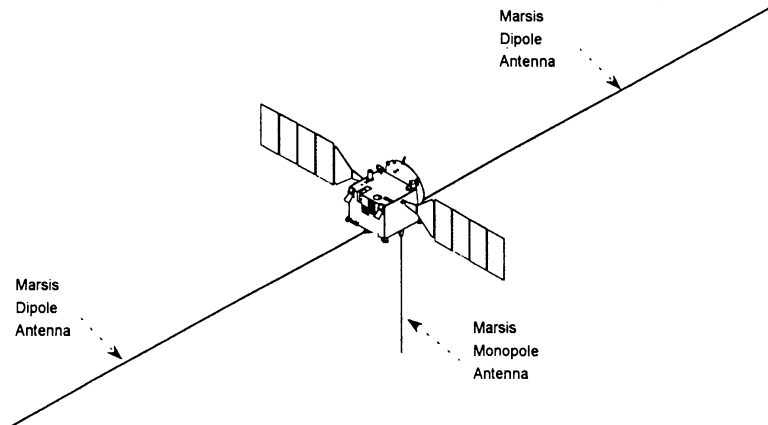


**Fig. 4. MARSIS**

Geometry and mass data relevant for the operational scenario after the Mars orbit injection are given in table 1 (Solar array and MARSIS antennae deployed).

**Table 1. Baseline geometry and mass properties after MOI**

SA surface	12 m <sup>2</sup>
Offset SA axis- CoM	0.62 m.
Mass	752 kg.
$I_x$ wrt CoM	839 kg.m <sup>2</sup>
$I_y$ wrt CoM	1196 kg.m <sup>2</sup>
$I_z$ wrt CoM	1848 kg.m <sup>2</sup>

Attitude and orbit control is achieved using star sensors, gyros, accelerometers and reaction wheels.

### 3.1. Reaction wheels.

The reaction wheels provide control torques to the AOCS for all phases of the mission except for trajectory corrections, the attitude acquisition and the backup modes. A wheel kinetic capacity from -12 Nms to +12 Nms enables to counteract all the disturbing torques and perform all the attitude manoeuvres during the scientific phase of the mission. The wheels are different to those of Rosetta but off-the-shelf units.

There are four reaction wheels placed in the tetrahedral configuration shown in fig.5

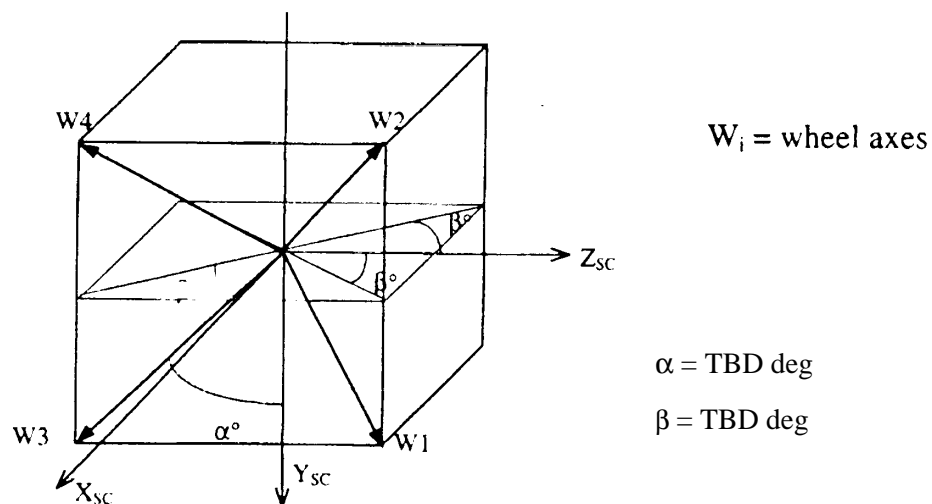


**Fig. 5. Reaction wheel configuration**

This configuration allows to cover the failure of one wheel among four: the system can still produce torque in any direction.

### 3.2. Reaction Control System

The number of reaction control thrusters has been limited to 8 (4 nominal and 4 redundant). They are located on the bottom (-Z) side of the S/C and they provide principally thrust in the Z direction to compensate main engine thrust imbalance, main engine misalignment and CoM uncertainties. They are adequately tilted (10 deg) in order to provide torques in any of the S/C axes. The thruster configuration is shown in figure 6.

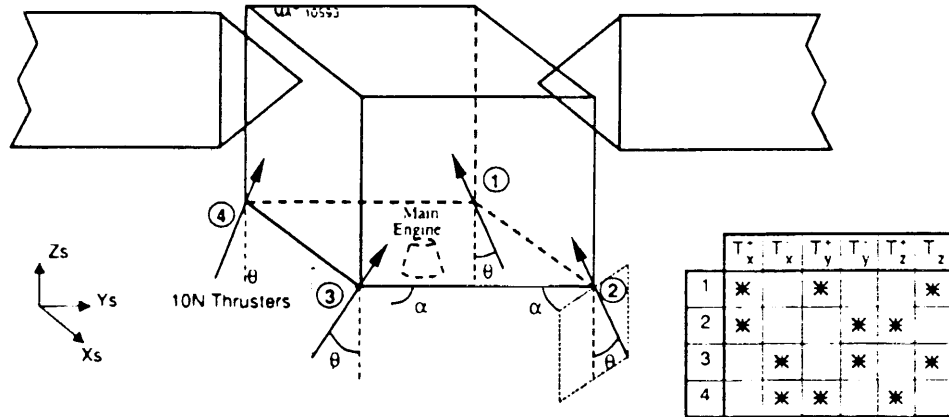


**Fig. 6. Thrusters disposition**

Note that it is not possible to generate pure forces in any direction other than the Z axis. It is also not possible to generate pure torques in any direction. Table 2 summarises the efficiency of the thruster configuration for the selected values of tilt and canting (ref.4)

**Table 2. RCS performances**

$\theta$ angle	$\alpha$ angle	$T_x$ [Nm]	$T_y$ [Nm]	$T_z$ [Nm]	$F_z$ [N]	$F_x$ [N]	$F_y$ [N]
10°	230 °	18.7	12.4	3.7	39.4	2.7	2.2
Thrusters activated:		1 & 2	1 & 4	2 & 4	all	1 & 4	1 & 2

Although the Mars Express propulsion system is a bi-propellant system, the densities, mix ratio and tank configuration are such that the propellant barycentre lies approximately on the S/C Z axis during the whole mission.

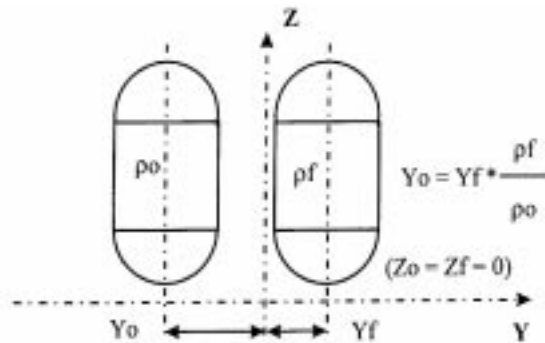


**Fig. 7. Propellant tanks configuration**

#### 4. OPERATIONAL ORBIT

An orbit of the G3 type has been selected as operational orbit (ref.1). The G3 orbits are characterised by an initial pericentre on the sun side, apocentre altitudes from 9800 to 11600 and inclination above 85 deg. A combination of two of them has been selected (G3ub = G3u for nominal operations + G3b for extended mission). The selection constitutes a compromise between day side viewing at low altitude demands from optical instruments and MARSIS demands which prefers night side observations.

The pericentre motion is tuned to obtain the best possible day and night side viewing conditions above both poles. The pericentre will be on the night side for about 38% of the time during the first martian year.

The apocentre has been tuned to get an adequate ground track spacing as required by optical instruments and to obtain a regular communications pattern with landers.

The first orbits after MOI are going to be taken as example cases in next sections. Some parameters of the orbit after the Mars Orbit Injection sequence are given in table 3 and are also representative for the first orbits:

**Table 3. Parameters<sup>1</sup> of the Orbit after MOI.**

Mean semimajor axis	$a = 9302 \text{ km}$
Mean eccentricity	$e = 0.606$
Mean pericentre altitude	$h_p = 270 \text{ km}$
Mean apocentre altitude	$h_a = 11549 \text{ km}$
Mean inclination	$i = 86.35 \text{ deg}$
Mean period	$T = 7.6 \text{ h} = 0.32 \text{ d}$

#### 5. ATTITUDE DEFINITION DURING THE ROUTINE OPERATIONS PHASE

The one degree of freedom of the solar array in Mars Express will allow pointing the HGA antenna towards the Earth or the line of sight of the instruments towards Mars and still keeping maximum power on the solar panels. Apart from the specific attitude required for delta-V manoeuvre (where the Z axis must be pointed in the desired thrust direction) four operational attitudes will be used commonly:

- Mars nadir pointing: the Z axis, where scientific instruments are mounted, is pointed towards the nadir. This attitude is used during the observation arc around the pericentre.
- Earth pointing attitude: The -X axis (assumed as HGA boresight) is pointing to Earth. This attitude will be used to allow high rate communications via the HGA to the Earth.
- Inertial attitude pointing to sun or stars, when required by SPICAM.
- Lander pointing, when communications with landers is required.

The last two attitudes are not considered in this study. In line with the preliminary character of this study and in

---

<sup>1</sup>. The inclination is wrt the Mars equator.

the interests of simplicity the attitude change manoeuvres between observation mode and communication mode are neither taken into account.

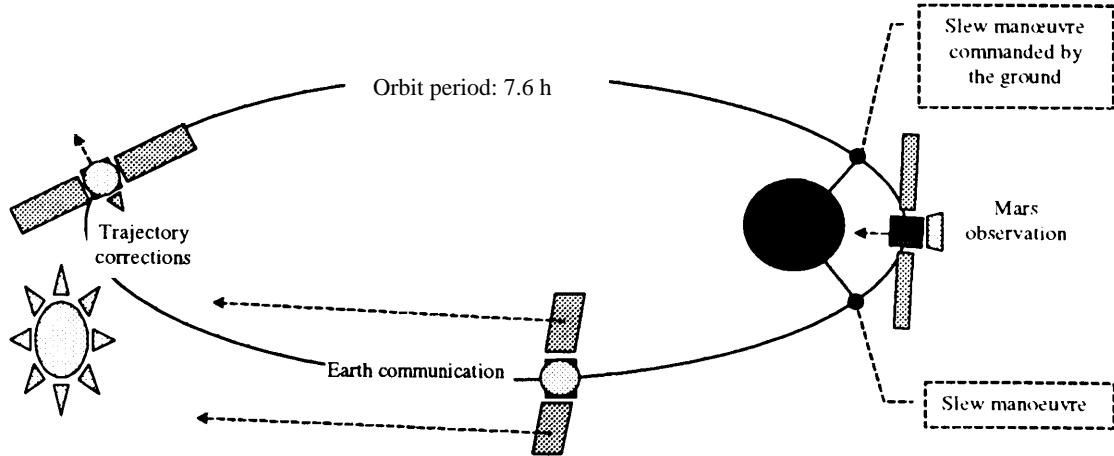


**Fig. 8. Scientific Phase Overview**

All the results of this document have been generated for two values of the limits on the maximum altitude of the observation phase: 1200 km and 4000 km.

For a complete description of the attitude evolution during the phases of interest the S/C rates are also calculated in Appendix III.

### 5.1. Nadir-pointing attitude

During the observation phase the Z axis of the spacecraft is pointing to nadir and therefore:

$$\vec{e}_z = -\frac{\vec{r}}{|\vec{r}|} \quad (1)$$

where  $\vec{r}$  is the position of MEX relative to Mars. This single condition does not fix the attitude completely since a rotation around this direction is still possible.

The performance of the camera pictures requires to maintain the X-axis perpendicular to the groundtrack and therefore:

$$\vec{e}_x = \pm \frac{\vec{r} \times (\vec{v} - \vec{\Omega} \times \vec{r})}{|\vec{r} \times (\vec{v} - \vec{\Omega} \times \vec{r})|} \quad (2)$$

Where  $\vec{v}$  is the MEX velocity relative to a Mars-fixed inertial frame and  $\vec{\Omega}$  is the Mars rotation velocity. The sign in eq.2 is chosen such that the radiators on the +X side are protected from sunlight, i.e.:

$$\vec{e}_x \cdot \vec{s} < 0 \quad (3)$$

where  $\vec{s}$  is the unit vector in the sun direction from MEX.

The Y-axis is defined by:

$$\vec{e}_y = \vec{e}_z \times \vec{e}_x \quad (4)$$

Note that in general the Y-axis is aligned neither with the vector  $\vec{v}$  nor with the vector  $\vec{v} - \vec{\Omega} \times \vec{r}$ .

As shown previously, during the observation the S/C Y-axis direction is fixed by operational requirements. This does not allow for keeping the solar array perpendicular to the sun direction. On the other hand, during

this phase, and in order not to perturb the instruments operations, the solar panels cannot be rotated. The orientation of the solar array must be selected at the entrance of the observation phase and maintained constant wrt the S/C during the whole arc. The selected orientation must be such that the total energy generated in the SA during this arc is maximised in order to reduce the batteries discharges. This leads to maximise the following integral extended along the part of the observation arc free of eclipses (ref.1):

$$E = \int_{noeclipse} \vec{n}_{SA} \cdot \vec{s} dt \quad (5)$$

where  $\vec{s}$  is the unit vector in the sun direction and  $\vec{n}_{SA}$  the unit vector normal to the solar array. This vector is perpendicular to the Y-axis (SA axis). Thus, it can be rewritten as:

$$\vec{n}_{SA} = \cos\Theta \vec{e}_z + \sin\Theta \vec{e}_x \quad (6)$$

where  $\Theta$  is the optimization variable defining the solar panel orientation at the entrance of the observation arc. Thus eq.5 may be expressed as:

$$E = \cos\Theta \underbrace{\int_{noeclipse} \vec{e}_z \cdot \vec{s} dt}_A + \sin\Theta \underbrace{\int_{noeclipse} \vec{e}_x \cdot \vec{s} dt}_B \quad (7)$$

The results of the optimization are (ref.1):

$$\Theta_{max} = \arctan\left(\frac{B}{A}\right) \Rightarrow E_{max} = \sqrt{A^2 + B^2} \quad (8)$$

where A and B are respectively the integrals that appear on eq. 7. For the purposes of this technical note these integrals for an orbital period can be evaluated at a first approach assuming keplerian orbit. This leads to analytical closed form expression of the optimal value, as developed in Appendix I.

## 5.2. Earth-pointing attitude

This mode corresponds to the rest of the orbit and is used to send data acquired during the observation arc to the Earth through the HGA. For the linking the -X axis is directed along the Earth direction i.e.:

$$\vec{e}_x = \frac{\vec{r}_E}{|\vec{r}_E|} \quad (9)$$

where  $\vec{r}_E$  is the position of MEX relative to Earth.

This guarantees that +X-side is protected from sunlight even when the angle between Earth and sun from MEX is maximum (quadrature) as shown in fig.9.

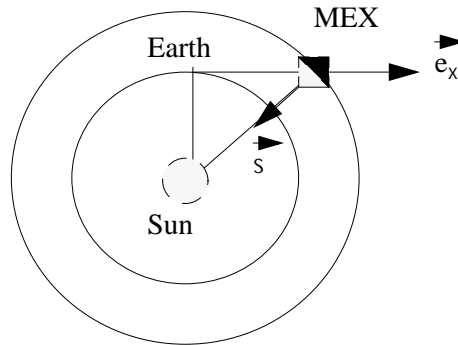


**Fig. 9. Sun-Earth-Mars quadrature.**

In order to maximize the power supplied the Y-axis is maintained perpendicular to the sun direction:.

$$\hat{e}_y = \pm \frac{\vec{r}_E \times \vec{s}}{|\vec{r}_E \times \vec{s}|} \quad (10)$$

The sign is chosen such that the sum of the angles of rotation from the last and to the next nadir-pointing mode is minimum.

The Z-axis unit vector completes the right-handed reference system.

$$\hat{e}_z = \hat{e}_x \times \hat{e}_y \quad (11)$$

The so defined attitude of the communication mode is quasi-inertial since the relative positions of Earth and sun wrt MEX do not change significantly throughout an orbit.

## 6. DISTURBANCE TORQUES

Perturbations due to gravity gradient and solar pressure are considered separately and analyses of torque disturbances and momentum loading per orbit are given for each case. The first orbit after the Mars orbit insertion sequence is chosen to show representative results.

The magnetic field of Mars is so low that no magnetic disturbance torque has been considered. The effect of the aerodynamic torque on the momentum loading is also negligible, as shown in section 6.3.

### 6.1. Gravity Gradient Torque

The following model for the gravity gradient torque has been adopted (ref.7):

$$\vec{T}_{gg} = \frac{3\mu}{r} \hat{u} \times \bar{I} \hat{u} \quad (12)$$

where:

$r$  is the distance from MEX to Mars center,

$\hat{u}$  is the nadir-pointing unit vector,

$\mu$  is the Mars gravitational constant ( $\mu = 42828 \text{ km}^3/\text{s}^2$ ),

$\bar{I}$  is the MEX inertia tensor.

The main inertia directions are basically along the S/C axes. Therefore the inertia tensor is assumed diagonal in S/C axes and no gravity gradient torque appears during the observation period (Z-axis nadir pointing) (see figs.10,11,12 and13). The values of the principal moments of inertia are given in table1.

The evolution of the gravity gradient torque is shown in fig.10 for an observation below an altitude limit of 4000 km and in fig.11 for an observation below 1200 km. The interval holds more than two periods ( $T = 7.6 \text{ h}$ ) to show explicitly the repetitiveness of the first orbit pattern. As mentioned before, the nil torques correspond to the nadir-pointing period around the pericentre ( $t = 0 \text{ h}, 7.6 \text{ h}, 15.2 \text{ h}$ ). Around the apocentre the torque magnitude is low since the distance  $r$  is maximum. The peak values take place on the extremes of the communication period and the rapid changes are due to the omission of transition manoeuvres.

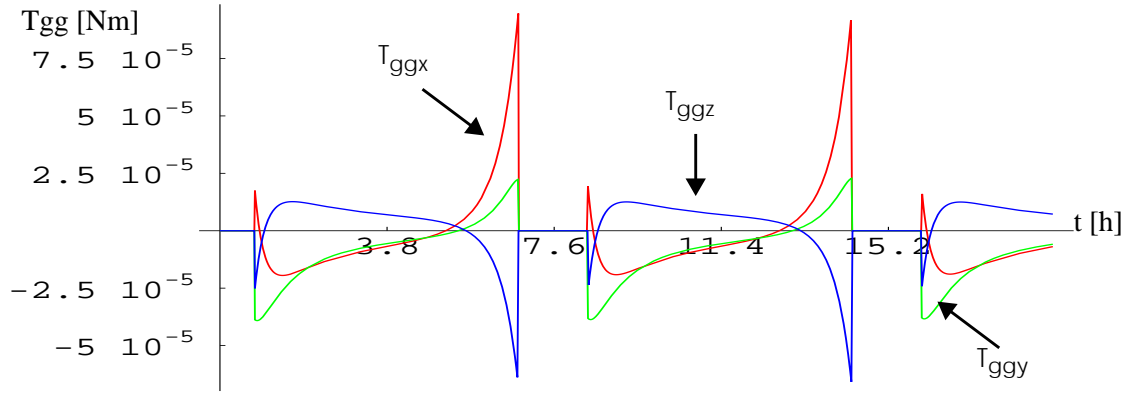


**Fig. 10. Gravity gradient torque along J2000 frame ( $h_0=4000$  km)**

For an observation below 1200 km the evolution is similar (see fig.11). The observation period around the pericentre is shorter and the gravity gradient peaks higher.

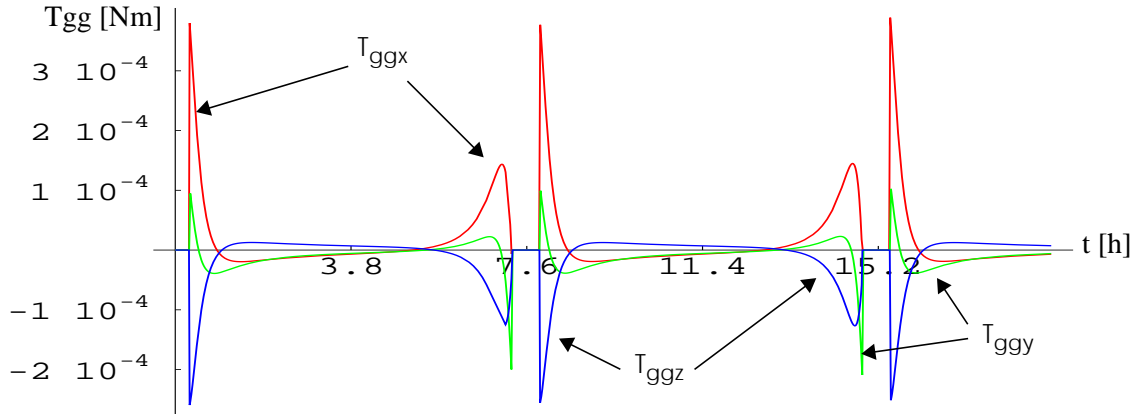


**Fig. 11. Gravity gradient torque along J2000 frame ( $h_0=1200$  km)**

The evolution of the gravity gradient torque on S/C axes has been also generated for the first orbit, which is representative enough of the next orbits.

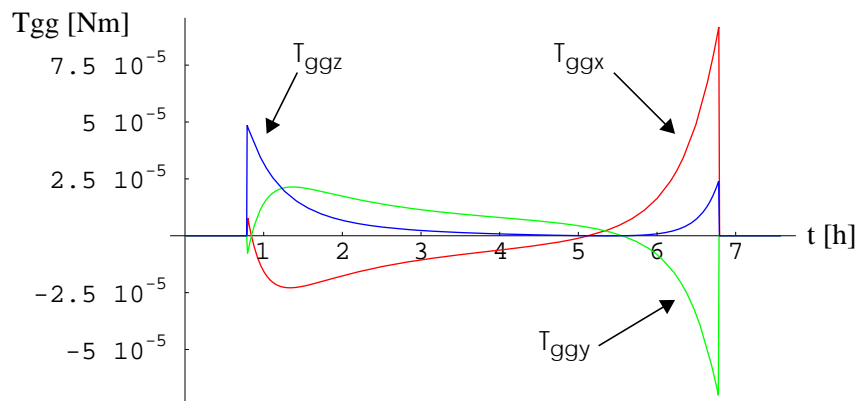


**Fig. 12. Gravity gradient torque in S/C axes ( $h_0=4000$  km)**

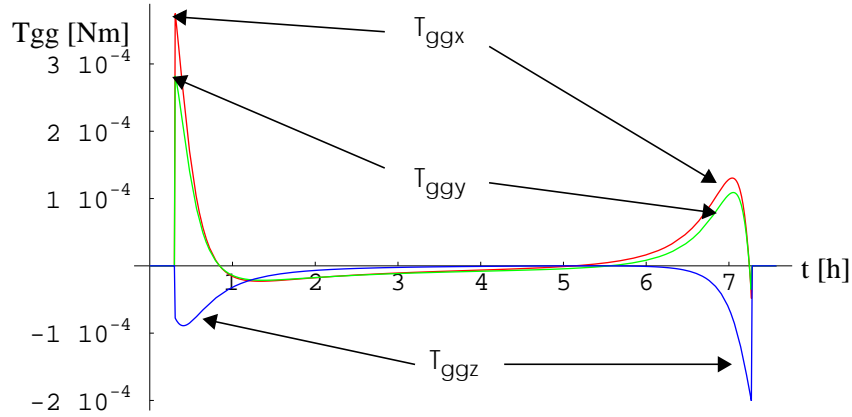


**Fig. 13. Gravity gradient torque in S/C axes ( $h_0=1200$  km)**

The momentum loading is the time integral over the disturbance torque in inertial axes. Appendix 2 shows how this integral may be approached by an analytical close-form for the gravity gradient torque contribution. The momentum loading caused by the gravity gradient in the first orbit is given in table 4:

**Table 4. Gravity gradient momentum loading per orbit in J2000 axes**

[Nms]	$\Delta H_x$	$\Delta H_y$	$\Delta H_z$	$\Delta H_{gg}$
$h_0 = 4000$ km	-0.004	-0.157	0.035	0.161
$h_0 = 1200$ km	0.470	-0.201	-0.362	0.626

Note that in case of the lower altitude limit for the observation period the loading is different in direction and remarkably higher in magnitude. This is due to the large contribution of the gravity gradient between 1200 and 4000 km as shown in the fig.14.

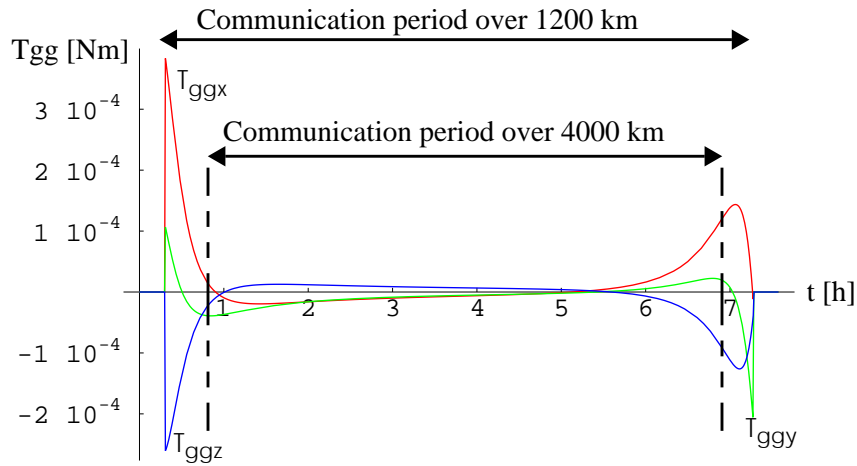


**Fig. 14. Gravity gradient torque comparison (J2000 axes)**

## 6.2. Solar Pressure Torque

The offset between SA axis and CoM is important (cf. section 2). The solar pressure torque is:

$$\vec{T}_{sp} = \vec{R} \times \vec{F}_{sp} \quad (13)$$

where  $\vec{R}$  is the lever arm or vector from the CoM to the center of pressure (CoP). No shadowing effects are considered and no contribution of the central body to the solar pressure torque is assumed at first approach. Therefore the CoP is assumed in the middle of the SA axis and the arm is along the direction of the S/C Z-axis.

$\vec{F}_{sp}$  stands for the total pressure force acting on the solar array, which is caused by absorption, specular reflection and diffusion effects (eqs. 14 to 17):

$$\vec{F}_{sp} = \vec{F}_{abs} + \vec{F}_{ref} + \vec{F}_{dif} \quad (14)$$

$$\vec{F}_{abs} = -PSC_a(\hat{s} \cdot \vec{n}_{SA})\hat{s} \quad (15)$$

$$\vec{F}_{ref} = -2PSC_s(\hat{s} \cdot \vec{n}_{SA})^2\vec{n}_{SA} \quad (16)$$

$$\vec{F}_{dif} = -PSC_d(\hat{s} \cdot \vec{n}_{SA})\left(\hat{s} + \frac{2}{3}\vec{n}_{SA}\right) \quad (17)$$

where:

$S$	is the solar array surface,	
$\hat{s}$	is the unit vector in the sun direction,	
$\vec{n}_{SA}$	is the unit vector normal to the solar array,	
$C_a$	is the optical absorption coefficient	( $C_a = 0.70$ TBC),
$C_s$	is the specular reflection coefficient	( $C_s = 0.24$ TBC),
$C_d$	is the optical diffusion coefficient	( $C_d = 0.06$ TBC),
$P$	is the solar pressure at 1.5 AU from the sun	( $P = 4.6 \mu\text{Pa} / 1.5^2$ )

The product  $S(\hat{s} \cdot \vec{n}_{SA})$  represents the effective solar array surface. For the observation period the solar array orientation must be selected at the entrance of this phase and maintained constant wrt the S/C during the whole arc. A closed-form analytical method to determine this orientation is developed in appendix I. Anyway the contribution of this phase to the solar pressure loading is quite low wrt the communication phase.

During the communication period the SA is perpendicular to the sun direction. Thus the SA normal and the sun direction coincide and the solar pressure force acts along this direction. As the CoP-CoM offset lies on the Z-axis, the solar pressure torque results aligned with the S/C Y-axis and its magnitude is constant, as shown in table 5 for the first orbit.

**Table 5. Solar pressure torque in the communication phase**

[Nm]		$T_{spX}$	$T_{spY}$	$T_{spZ}$
$h_o = 4000$ km	S/C axes	0	$1.36 \cdot 10^{-5}$	0
	J200 axes	$-2.98 \cdot 10^{-8}$	$-5.43 \cdot 10^{-6}$	$1.25 \cdot 10^{-5}$

The magnitude of the solar pressure torque during the Earth-Pointing phase is logically the same for the case of a limiting observation altitude of 1200 km. This interval during which the torque is acting is however longer. The momentum loading caused by the solar pressure in the first orbit is given in table 6.

**Table 6. Solar pressure momentum loading per orbit in J2000 axes:**

[Nms]	$\Delta H_x$	$\Delta H_y$	$\Delta H_z$	$\Delta H_{sp}$
$h_o = 4000$ km	-0.008	-0.105	0.258	0.279
$h_o = 1200$ km	-0.006	0.148	-0.327	0.359

The differences between the two observation cases are not so marked as in the previous subsection. During the communication phase, the directions of Y-axis and Z-axis for the case  $h_o=4000$  km are opposed to the case of  $h_o=1200$  km. This is a consequence of the determination of sign in eq.10.

Note that the solar pressure momentum loading is 73% greater than gravity gradient for the limit of 4000 km. However the contribution of solar pressure is just a 57% of the gravity gradient momentum loading for the case of 1200 km.

### 6.3. Aerodynamic torque

As a first approach the aerodynamic torque can be modelled in a similar way to the solar pressure torque:

$$\vec{T}_{ad} = \frac{1}{2} \rho S |\vec{v} \cdot \vec{n}_{SA}| C_D \vec{v} \times \vec{R} \quad (18)$$

where:

$\vec{R}$  is the lever arm or vector from the CoM to the center of pressure (CoP),

$C_D$  is the aerodynamic drag coefficient,

$\rho$  is the atmospheric density corresponding to a given position over Mars (by Mars-Gram model).

$\vec{v}$  is the velocity of MEX relative to the local Mars atmosphere.

The term  $S |\vec{v} \cdot \vec{n}_{SA}|$  represents the product of the speed and the effective solar array surface.

Only during some minutes around the pericentre passage (altitude 270 km) the magnitude of the aerodynamic torque should be taken into account. However the duration of this interval is so short that the effect on the overall momentum loading per orbit is neglected. (An estimation for the first orbit yields only -0.004 Nms).

## 7. REACTION WHEELS OFF-LOADING

The evolution of the total disturbance torque is depicted in figs.15 and 16 for the first orbit after MOI sequence. The next orbits are alike and describe a very similar pattern of disturbance torque and therefore of angular momentum loading.

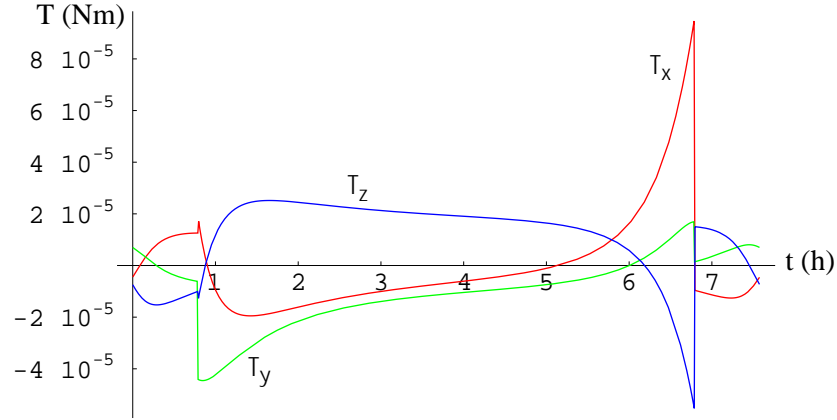


**Fig. 15. Total disturbance torque along J2000 frame ( $h_0=4000$  km)**

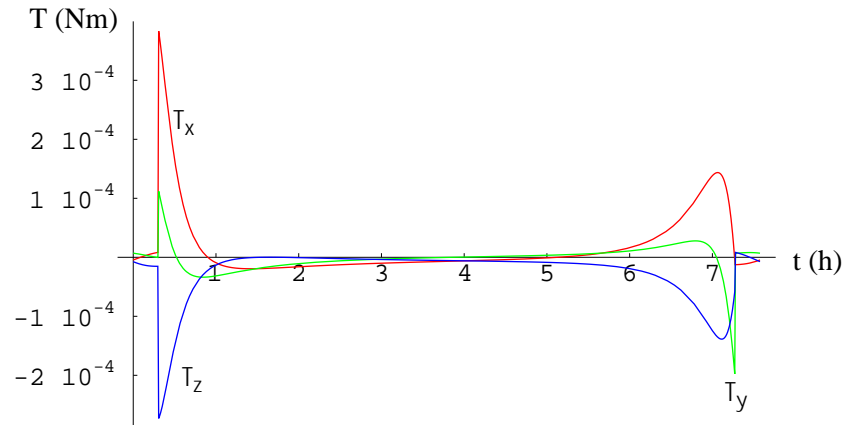


**Fig. 16. Total disturbance torque along J2000 frame ( $h_0=1200$  km)**

The momentum loading is the time integral over the total disturbance torque in inertial axes:

$$\Delta \vec{H}(t) = \int_{t_o}^t \vec{T}(\tau) d\tau \quad (19)$$

Its evolution for the case of a limiting observation altitude of 4000 km is shown in fig.17 ( $T=0.32$  d)

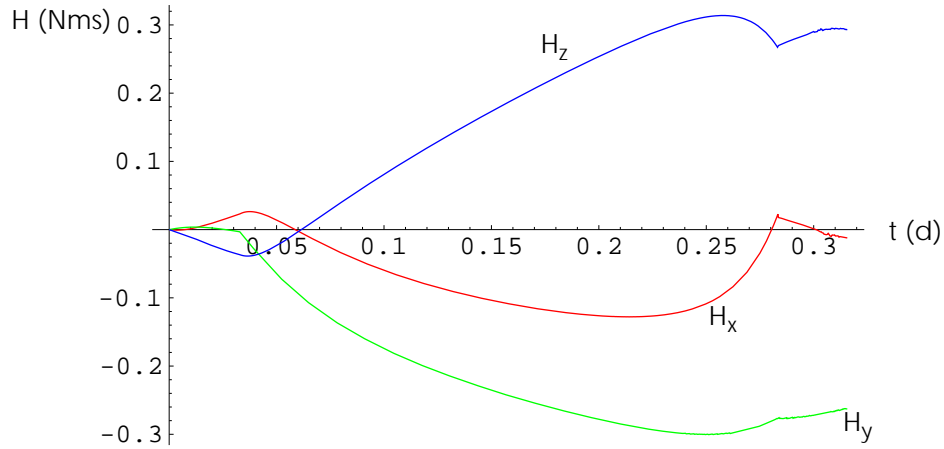


**Fig. 17. Momentum loading throughout an orbit along J2000 frame ( $h_o=4000$  km)**

An analytical approach to compute the contribution of the gravity gradient has been developed in Appendix II.

The total angular momentum accumulated on the first orbit is given in table 8:

**Table 7. Total momentum loading per orbit in J2000 axes**

[Nms]	$\Delta H_x$	$\Delta H_y$	$\Delta H_z$	$\Delta H$
$h_o = 4000$ km	-0.012	-0.263	0.293	0.394
$h_o = 1200$ km	0.463	-0.052	-0.688	0.831

Note than for the second case the loading per orbit is significantly higher mainly because of the contribution of the gravity gradient torque between 1200 km and 4000 km.

### 7.1. Schedule of time slots for wheel off-loading

The disturbance torques load the reaction wheels. The reactions wheels have a limited capacity and before becoming saturated must be off-loaded. Off-loadings during observation period are avoided. The real planning of time slots for wheel off-loading should also consider other aspects such as Perth ground station coverage, orbit perturbation and margin of RW for other manoeuvres and avoidance of zero-crossing. Off-loading manoeuvres may be divided in few thrusters actuations to remain compatible with RW capability, to limit excitation of MARSIS antennae and to ensure that Earth-communications are not interrupted.

For the next sections RW off-loading in the communication period after accumulation of about 5.5 Nms is assumed as a preliminary strategy consistent with the purposes of this study. For the first orbits after MOI the off-loadings would then take place approximately once every 4.4 days for the case of 4000 km and every 2.1 days for the case of 1200 km.

The resulting angular momenta to off-load at the first slot are the input for the determination of the thrusters actuation. The angular momentum in the S/C axes (Earth-pointing attitude) at the first slot is shown in table 8.

**Table 8. Angular momentum at first off-loading slot in body axes**

[Nms]	$\Delta H_x$	$\Delta H_y$	$\Delta H_z$
$h_o = 4000 \text{ km}$	-0.487	4.668	1.481
$h_o = 1200 \text{ km}$	2.121	3.365	-2.257

## 7.2. Off-Loading Strategies

Different combinations of attitude manoeuvres and thrusters activation can desaturate the reaction wheels with different fuel consumption, different orbit perturbation (residual delta-v) and different manoeuvre duration. Also the HGA off-pointing and the solar incidence on the SA depend on the off-loading strategy.

Procedures are presented in the following and applied to the first off-loading slot as an example.

### 7.2.1. Off-loading from the communication attitude

If the off-loading is carried out directly from the communication attitude, the solar incidence on the S/C is adequate. In this case the duration of the off-loading is only set by the time of actuation of the RCS and the following tranquillisation phase, as prescribed by the Off-loading Mode (ref.13).

Through the actuation of the thrusters a torque is generated opposite to the accumulated angular momentum. The time of actuation is such that this momentum loading is counteracted. This is established in expr. 20:

$$-\Delta \vec{H} = \sum_{i=1}^n \dot{\vec{r}}_i \times s_{Ii} \vec{e}_i = \left[ \dot{\vec{r}}_1 \times \vec{e}_1, \dots, \dot{\vec{r}}_n \times \vec{e}_n \right] \vec{s}_I = E_T \vec{s}_I \quad (20)$$

where:

$\dot{\vec{r}}_i$  is the position of thruster i wrt the CoM of MEX. For the second thruster it is (0.81,0.72,-0.58) (m) in S/C axes. The others are laid out symmetrically wrt XZ and YZ planes (section 3.2)

$n$  is the number of thrusters (4),

$s_{Ii}$  is the impulse (Ns) generated by thruster i.

$\vec{e}_i$  is the unit vector in the direction of the thruster i,

$E_T$  is the action matrix to compute torque or angular momentum generated by the RCS,

$\Delta \vec{H}$  is the angular momentum to be off-loaded, given in table8.(Nms)

$\vec{s}_I$  is a vector whose four components  $s_{Ii}$  are the required impulses of each thruster ( $s_{Ii}$  must be positive). Therefore it is determined by solving the linear set of equations from expression 20 as shown in eq.21:

$$\vec{s}_I = \vec{s}_o + \sum_{j=1}^m \lambda_j \vec{s}_{N_j} \quad (21)$$

where:

$\vec{s}_o$  is a particular solution of the set,

$\vec{s}_{N_j}$  is a vector base of the kernel or null space of  $E_T$ ,

$\lambda_j$  is a free parameter,

$m$  is the dimension of the kernel or null space of  $E_T$ .

Because of the symmetrical configuration of the RCS wrt the CoM the actuation of the four thrusters with the same impulse generates just a force along the Z-axis without any torque. This is the only way to produce a pure force. It means that the dimension of the kernel of the torque action matrix  $E_T$  is one ( $m=1$ ) and a representative vector of the kernel  $\dot{s}_N$  is  $[1 \ 1 \ 1 \ 1]$ . Thus there is one degree of freedom on the solution:

$$\dot{s}_I = \dot{s}_o + \lambda [1 \ 1 \ 1 \ 1]^T \quad (22)$$

and an additional condition must be imposed to fix the thruster actuation, for instance, the minimization of fuel consumption.

Since no pure torque can be generated by the MEX RCS, a residual impulse  $\dot{I}$  appears in any case, given by eq. 23:

$$\dot{I} = \sum I_i \dot{e}_i = [\dot{e}_1 \mid \dot{e}_2 \mid \dots] \{\dot{s}_I\} = E_F \dot{s}_I \quad (23)$$

where  $E_F$  is the action matrix to compute forces or impulses by the reaction control system. The minimum fuel consumption corresponds to the minimum sum of the impulses of all the thrusters:

$$\text{Min}(\sum I_i) \Rightarrow \dot{s}_I = \dot{s}_o - \text{Min}(s_{o_i}) [1 \ 1 \ 1 \ 1]^T \quad (24)$$

This solution sets the parameter  $\lambda$  as the opposite of the minimum component of the particular solution  $\dot{s}_o$ . In other words, part of the actuation of the thrusters that does not contribute to the torque is subtracted. The result is that only three thrusters need to be switched on as depicted in fig.18.

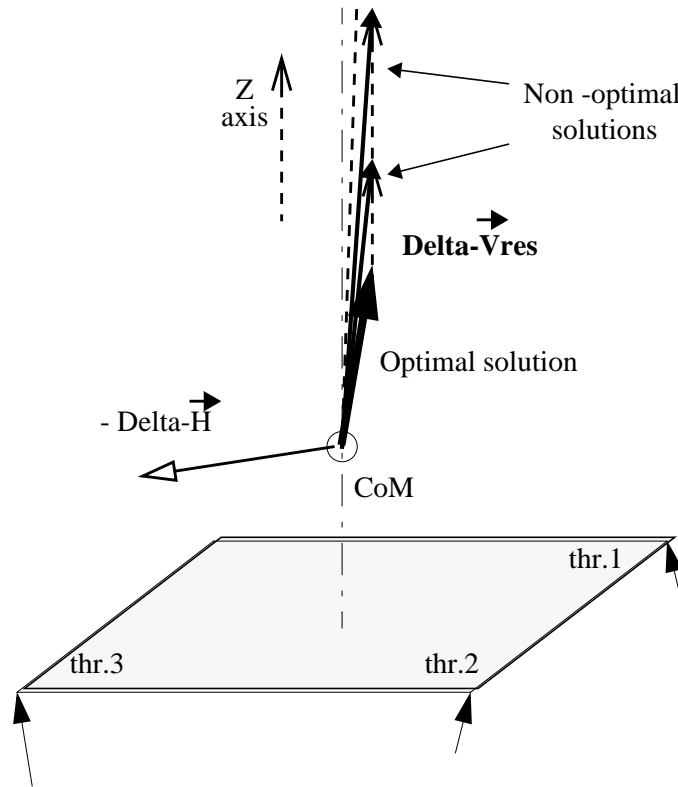


**Fig. 18. Off-loading without rotation (Sketch)**

We state without proof, that for the MEX RCS configuration this solution provides also the minimum delta-v, given by expression 25.:

$$\Delta \vec{v}_{res} \approx \frac{\dot{\vec{I}}}{M_{MEX}} = \frac{E_F \dot{s}_I}{M_{MEX}} = \frac{E_F \dot{s}_o}{M_{MEX}} - \underbrace{Min(s_{oi}) \frac{E_F \dot{s}_N}{M_{MEX}}}_{|| \vec{e}_z} \quad (25)$$

where  $M_{MEX}$  is the mass of Mars Express assumed as practically constant during this manoeuvre.

Numerical application to the first off-loading slot is shown in table 9. The resulting impulse is mainly along S/C Z-axis, as corresponding to the slightly tilted RCS configuration (see fig. 6)

**Table 9. Off-loadings results<sup>1</sup> at first slot (I) ( $h_o=4000$  km)**

Thuster actuations	i	thruster 1	thruster 2	thruster 3	thruster 4
	Impulse (Ns)	4.197	3.386	6.954	0.
	On -time (s)	0.420	0.339	0.695	0.

OVERALL ACTIONS		X	Y	Z
Angular momentum (Nms)	S/C axes	0.487	-4.668	-1.481
	J2000 axes	0.152	3.285	-3.661
Impulse (Ns)	S/C axes	-0.817	0.070	14.317
	J2000 axes	2.474	-12.986	-5.556
Delta-V (m/s)	J2000 axes	0.003	-0.017	-0.007

### 7.2.2. Activation of just one thruster with the minimum S/C rotation

According to the previous section, if the off-loading is performed directly from the initial communication attitude three thrusters need to be activated in general.

However the S/C attitude can be free in principle with the single condition of generating a torque opposed to the accumulated momentum. In this case certain attitudes are possible such that the activation of just one thruster suffices to provide the required torque. It can be shown that these strategies lead to the minimum fuel consumption and to the minimum residual force. Sections 7.2.2 and 7.2.3 describe these attitudes and how to achieve them from the initial Earth-pointing attitude corresponding to the communication period.

<sup>1</sup>. On-time as net actuation duration of thruster at max. level (10 N).

In this section the off-loading attitude is also selected such that the manoeuvre from the initial (Earth-pointing) attitude is minimised. Constraints on solar incidence are considered a posteriori.

As mentioned above, a rotation of the spacecraft is required in order to place the torque of a single thruster "i" opposite to the angular momentum to off-load. It means that the plane defined by the position of the thruster  $\vec{r}_i$  and the direction  $\vec{e}_i$  of its thrust must be set perpendicular to the momentum  $\Delta\vec{H}$

The axis and the direction of this rotation is given by the unit vector in eq.26:

$$\vec{u}_r = \frac{(\vec{r}_i \times \vec{e}_i) \times (-\Delta\vec{H})}{|(\vec{r}_i \times \vec{e}_i) \times (-\Delta\vec{H})|} \quad (26)$$

From equation 27 the angle of rotation  $\phi$  of the S/C is determined.

$$\cos\phi = -\frac{\Delta\vec{H}}{|\Delta\vec{H}|} \cdot \frac{\vec{r}_i \times \vec{e}_i}{|\vec{r}_i \times \vec{e}_i|} \quad (27)$$

Hence the thruster "i" with the minimum angle of rotation may be chosen.

The change of attitude of the S/C is then completely defined. For instance, from the axis and the angle of rotation the quaternion of the transformation is easily determined.

Anyway the unit vector of the resulting impulse may be explicitly formulated (eq. 28),

$$\vec{e}_i^r = \cos\phi \vec{e}_i + (1 - \cos\phi)(\vec{e}_i \cdot \vec{u}_r)\vec{u}_r + \sin\phi \sqrt{1 - (\vec{e}_i \cdot \vec{u}_r)^2} \frac{\vec{u}_r \times \vec{e}_i}{|\vec{u}_r \times \vec{e}_i|} \quad (28)$$

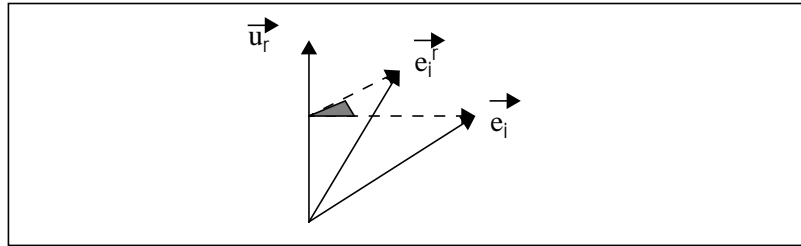


**Fig. 19. Rotation of the thrust direction (sketch)**

and the magnitude of the impulse is directly fixed by:

$$I = \frac{|\Delta\vec{H}|}{|\vec{r}_i \times \vec{e}_i|} \quad (29)$$

Numerical application to the first off-loading slot is shown in table 10. The impulse now required is more than three times lower than for the previous case (three thrusters&no pre-orientation rotation). Consequently the ratio of fuel saving per off-loading is remarkable (0.31). The reduction of the orbit perturbation is equally to be noted.

**Table 10. Off-loadings results<sup>1</sup> at first slot (II) ( $h_0=4000$  km)**

Initial S/C rotation angle		47.8 deg (as minimum value corresponding to thruster 2)			
Thuster actuations	i	thruster 1	thruster 2	thruster 3	thruster 4
	Impulse (Ns)	0.	4.469	0.	0.
	On -time (s)	0.	0.447	0.	0.
OVERALL ACTIONS		X	Y	Z	
Angular momentum	J2000 axes (Nms)	0.152	3.285	-3.661	
Impulse	J2000 axes (Ns)	1.265	-3.217	-2.833	
Delta-V	J2000 axes (m/s)	0.002	-0.004	-0.004	
Angle (sun direction, SA axis)		107.1 deg			
Angle (sun direction, X-axis)		143.6 deg			

The effected rotation changed the orientation of the S/C wrt the sun. Initially (communication mode attitude) the SA is perpendicular to the sun direction. Therefore the sun power and the solar incidence on the +/-Y-side are altered. Fortunately after this first off-loading slot the +X-wall remains protected from sunlight.

### 7.2.3. Activation of just one thruster with the best sun incidence

For a general case the activation of one thruster with minimum S/C rotation may lead to an incorrect sun incidence. Once the torque of a single thruster is placed opposite to the angular momentum to off-load, a degree of freedom is still available without altering the desaturation: a rotation of the S/C around the momentum direction. Accordingly the Y-axis describes a cone of possible positions (fig.20) around the momentum direction.

The aim is to determine the attitude of the best solar incidence, i.e. the direction of the Y-axis closest to 90 deg wrt the sun direction and keeping the X-side shadowed. In other words, the intersection of that cone and a plane perpendicular to the sun direction (containing the apex of the cone) (fig.28), or if not possible, the direction on the cone closest to this plane.

<sup>1</sup>. On-time as net actuation duration of thruster at max. level (10 N).

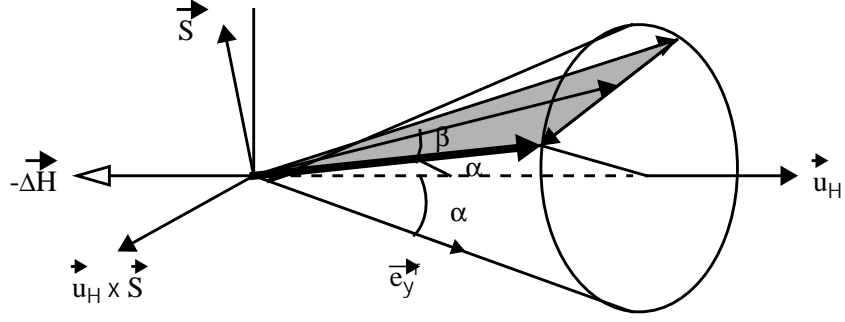


**Fig. 20. Y-axis determination**

The intersection is feasible if:

$$\left| \frac{\Delta \vec{H}}{|\Delta \vec{H}|} \times \vec{s} \right| \geq \cos \alpha \quad (30)$$

where  $\alpha$  is the semiangle of the cone. This is a characteristic of the RCS geometry given by:

$$\cos \alpha = \left| \vec{e}_y \cdot \frac{\vec{r}_i \times \vec{e}_i}{|\vec{r}_i \times \vec{e}_i|} \right| \quad (31)$$

For the MEX configuration this value is 0.69 ( $\alpha = 46.4$  deg) for any of the four thrusters since they are mounted symmetrically.

When it can be fulfilled, the condition of orthogonality to the sun direction leads to the following expression for the Y-axis:

$$\vec{e}_y^s = \pm \sin \beta \frac{\vec{u}_H \times \vec{s}}{|\vec{u}_H \times \vec{s}|} + \cos \beta \vec{s} \times \frac{\vec{u}_H \times \vec{s}}{|\vec{u}_H \times \vec{s}|} \quad (32)$$

where  $\vec{u}_H$  is the unit vector of the direction of rotation (along the angular momentum) given by:

$$\vec{u}_H = \text{Sign}(\Delta \vec{H} \cdot \vec{e}_y^r) \frac{\Delta \vec{H}}{|\Delta \vec{H}|} \quad (33)$$

$\vec{e}_y^r$  is the Y-axis direction of any of the S/C attitudes that fulfill the off-loading condition with the thruster "i", for instance, the resulting Y-axis after the minimum rotation manoeuvre from the previous subsection (eq.28).

The angle  $\beta$  is fixed by imposing that  $\vec{e}_y^s$  must be on the cone:

$$\vec{e}_y^s \cdot \vec{u}_H = \cos \alpha \quad (34)$$

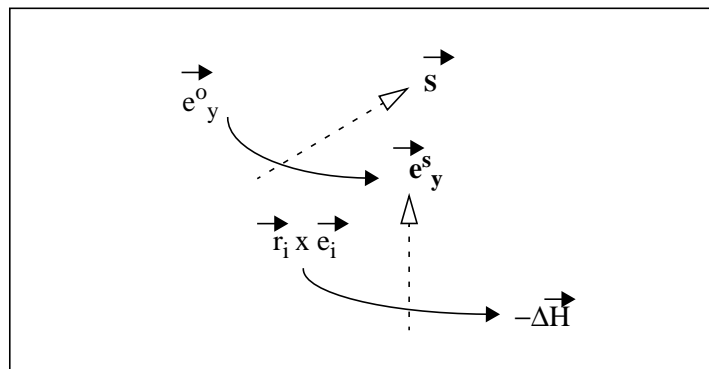
which yields:

$$\cos \beta = \frac{\cos \alpha}{|\vec{u}_H \times \vec{s}|} \quad (35)$$

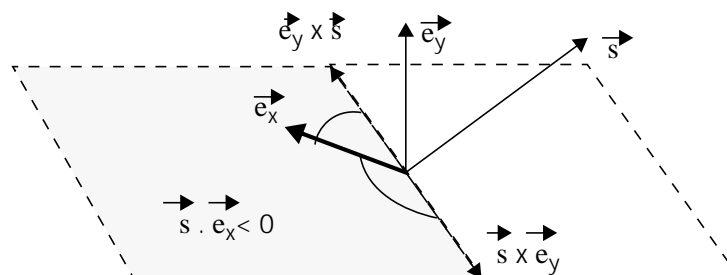
As depicted in fig.20 and as followed from eq.32 two solutions may be possible. If one of them leads to solar incidence on X-side then it will be discarded. On this respect if both are not suitable the same process with another thruster "i" will be carried out. In the limit case  $\cos \beta = 1$  only one solution is possible (the plane perpendicular to the sun direction is tangent to the cone).

$$\vec{e}_y^s = \cos \alpha \vec{u}_H - \text{Sign}(\vec{u}_H \cdot \vec{s}) \sin \alpha \frac{\vec{s} - (\vec{s} \cdot \vec{u}_H) \vec{u}_H}{|\vec{s} - (\vec{s} \cdot \vec{u}_H) \vec{u}_H|} \quad (36)$$

As mentioned above application may be done for every thruster. Off-loading attitudes that preserve sun-incidence within an admissible range are possible. To achieve them from the initial S/C attitude (Earth-pointing attitude) two rotations may be done, as indicated in fig.21. Firstly a rotation around the sun direction in order to fix the Y-axis direction (from eq.32 or from eq.36) without altering the sun incidence on the S/C. Then a rotation around this Y-axis to align the torque of the chosen thruster opposite to the angular momentum to off-load (in a similar way as in the previous subsection). Both rotations may be combined in a single manoeuvre: S/C rotation around the Y-axis (body-axis), which is being slewed around the sun direction (quasi-inertial axis).



The solar incidence on the X-side is only affected by the S/C turn around the Y-axis (fig.19)



Numerical application has been carried out for the first slot once again using only the second thruster (Table 11). Two solutions are feasible. The one corresponding to minimum angles has been chosen. Logically thruster actuations are the same and only the directions of impulse and delta-v are slightly different

**Table 11. Off-loadings results<sup>1</sup> at first slot (III) ( $h_0=4000$  km).**

Rotation around sun-direction	53.7deg
Rotation around Y-axis	12.5 deg

Thuster actuations	i	thruster 1	thruster 2	thruster 3	thruster 4
Impulse (Ns)		0.	<b>4.469</b>	0.	0.
On -time (s)		0.	0.447	0.	0.

OVERALL ACTIONS		X	Y	Z
Angular momentum	J2000 axes (Nms)	0.152	3.285	-3.661
Impulse	J2000 axes (Ns)	-0.912	-3.237	-2.943
Delta-V	J2000 axes (m/s)	-0.001	-0.004	-0.004

Angle (sun direction, SA axis)	<b>90 deg</b>
--------------------------------	---------------

Angle (sun direction, X-axis)	126 deg
-------------------------------	---------

#### **7.2.4. Treatment of the activation of two thrusters.**

This is an intermediate possibility between using three thrusters without attitude manoeuvre and rotating the S/C & activating only one thruster. The activation of a second thruster introduces an additional degree of freedom, making it easier to fulfil the solar incidence constraints. The pre-orientation manoeuvres may be shorter but the fuel consumption and orbit perturbation are worse than in the case of just one thruster activation.

Taking into account the configuration of the reaction control system of MEX, the combination of two thrusters that are not at the same side (e.g.1, 3) is very inefficient in terms of torque per fuel consumed. Therefore only activation of contiguous thrusters is considered here. In this case the lines of action of the thrusts intersect one another and the set of forces may be substituted by a resulting force acting at the intersection point, as shown in fig.23. Therefore the treatment is now equivalent to the case of one thruster. The degree of freedom on combining the two thrusters is translated into the ability of orienting the resulting thrust and, accordingly, the corresponding torque (fig.23).

<sup>1</sup>. On-time as net actuation duration of thruster at max. level (10 N).

As followed from the previous subsection, a correct sun incidence is more easily feasible if the semiangle of the cone of fig.20 is high, i.e. if the torque and the Y-axis are nearly perpendicular. Hence the combination of thrusters 1 & 2 is preferred rather than 1&4 or 2&3.

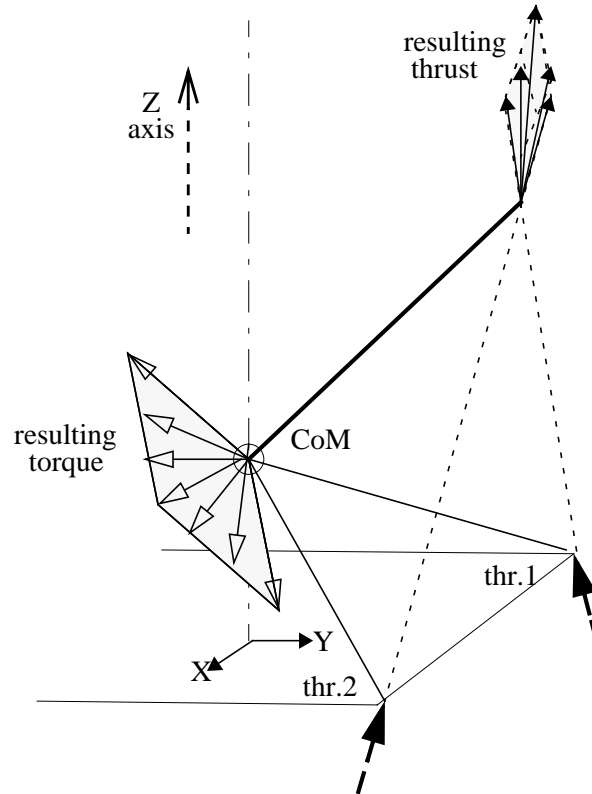


**Fig. 23. Reduction of two thrusters application**

When fixing for instance the same impulse for both thrusters 1 & 2 the torque is aligned with the S/C X axis, thus perpendicular to the Y-axis (the cone is transformed in a plane: two solutions are always possible). In this case numerical application to the first slot yields a fuel consumption and a residual  $\Delta V$  41.1% higher than in case of activation of just one thruster.

## 8. CONCLUSIONS

A preliminary analysis of the angular momentum loading due to disturbance torques and an indication of different off-loading strategies have been carried out. Some simplifications and illustrative results have been shown based on provisional data of the MEX spacecraft and parameters of the first operational orbits after Mars orbit insertion.

The MARSIS dipole antenna has a large impact on the inertia tensor of MEX and consequently on the gravity gradient torque results. Because of the significant offset between the SA axis center and the MEX CoM the solar pressure torque is also to be considered. For the first orbits after MOI the total angular momentum loading per orbit is about 0.4 Nms for a maximum altitude of observation of 4000 km. The loading is more than doubled when this top altitude is reduced to 1200 km mainly due to a more intense action of the gravity gradient.

The required off-loadings should take place in the communications period, about once every four days for the case of 4000 km as maximum altitude observation. Some advantageous off-loading strategies have been found after modelling the actions of the MEX reaction control system at different possible off-loading attitudes. It turns out feasible to desaturate the reaction wheels by activating just one thruster at certain attitudes that maintain a correct solar incidence on the S/C. This option allows for saving of about 69% of the fuel needed for the

nominal off-loading manoeuvres i.e. those performed directly from the initial (communication) attitude, which requires the activation of three thrusters in general. Including the extended operations phase an overall fuel saving of more than 1 kg may be reached.

Accordingly the residual forces are also reduced at the same ratio. Additionally, the residual delta-V from one off-loading can be largely counteracted by the residual delta-v from the next off-loading when performed by the same thruster from an attitude rotated 180 deg wrt the direction of the angular momentum.

The freedom in the choice of the thrusters to be activated and of the off-loading pre-orientation slew manoeuvre leads to different residual forces. These can be selected such that they are beneficial for the orbit maintenance. On the other hand, the residual torques from trajectory corrections manoeuvres could be matched to modify the S/C angular momentum conveniently if the MEX S/C had the capability to perform delta-v manoeuvres controlled by reaction wheels.

*The actual applicability of the proposed strategies is to be considered along with other system constraints, such as thermal constraints on +Z side (TBC), zero-crossing range of the reaction wheels (TBC), operational complexity and mission planing (TBC).*

## 9. APPENDIX I: SA ORIENTATION DURING NADIR-POINTING PHASE

As described in section 5.1, the determination of the orientation of the solar array (eq.37)

$$\vec{n}_{SA} = \cos\Theta \vec{e}_z + \sin\Theta \vec{e}_x \quad (37)$$

requires the evaluation of the integrals that appears in eq.38:

$$E = \cos\Theta \underbrace{\int_{noeclipse} \vec{e}_z \cdot \dot{\vec{s}} dt}_A + \sin\Theta \underbrace{\int_{noeclipse} \vec{e}_x \cdot \dot{\vec{s}} dt}_B \quad (38)$$

Consistent with the purposes of this study, a simplification has been carried out assuming keplerian orbit without any eclipse along the arc. Since the sun direction does not vary practically during one orbit the first integral is given in eq.39:

$$A = \int \vec{e}_z \cdot \dot{\vec{s}} dt \approx \dot{\vec{s}} \cdot \int \vec{e}_z dt \quad (39)$$

The nadir-pointing (or Z-axis) unit vector changes throughout the observation arc and it may be rewritten in terms of the true anomaly according to:

$$\vec{e}_z = -\cos v \vec{u}_P - \sin v \vec{u}_Q \quad (40)$$

where  $\vec{u}_P$  is the unit vector from Mars to the pericentre of the orbit and  $\vec{u}_Q$  is the perpendicular unit vector (fig. 24). Both of them are assumed constant during an orbit.

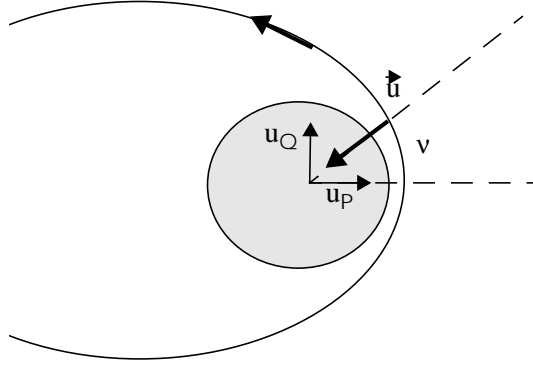


**Fig. 24. Nadir-pointing sketch**

The second term of the second member of eq.40 vanished when integrated along a symmetric arc around the pericentre. Therefore introducing eq.40 in eq.39 yields:

$$A \approx -\vec{s} \cdot \vec{u}_P \int \cos v dt \quad (41)$$

The integration is easier when in terms of the eccentric anomaly  $E$ .

$$\cos v = \frac{a(\cos E - e)}{r} \quad (42)$$

$$r = a(1 - e \cos E) \quad (43)$$

$$dt = \sqrt{\frac{a^3}{\mu}} (1 - e \cos E) dE \quad (44)$$

Thus, inserting eqs. 42, 43 and 44 into eq.41 yields:

$$A \approx -\vec{s} \cdot \vec{u}_P \sqrt{\frac{a^3}{\mu}} \int (\cos E - e) dE \quad (45)$$

i.e. integrating along the observation arc (symmetric around the pericentre) leads to:

$$A \approx -\vec{s} \cdot \vec{u}_P 2 \sqrt{\frac{a^3}{\mu}} [\sin E_f - e E_f] \quad (46)$$

where the final eccentric anomaly  $E_f$  is a function of the upper limit of the observation altitude  $h_{obs}$ , as shown in eq.47.

$$E_f = \arccos \left( \frac{1 - \frac{h_{obs} + R_{Mars}}{a}}{e} \right) \quad (47)$$

$R_{Mars}$  is the Martian radius.

The second integral of equation 38 can be computed assuming that the sun direction does not change significantly during the interval of integration:

$$B = \int \hat{e}_x \cdot \hat{s} dt \approx \hat{s} \cdot \int \hat{e}_x dt \quad (48)$$

where the X-axis<sup>1</sup> was defined as orthogonal to the groundtrack and to the nadir pointing direction (eq.2).

## 10. APPENDIX II: MOMENTUM LOADING BY GRAVITY GRADIENT TORQUE

An analytical approach is developed to compute the angular momentum loading due to the gravity gradient torque during the operational phase. The model for the gravity gradient torque is given in eq. 49:

$$\vec{T}_{gg} = \frac{3\mu}{r} \hat{u} \times \bar{I} \hat{u} \quad (49)$$

where:

- $r$  is the distance from MEX to Mars center,
- $\hat{u}$  is the nadir-pointing unit vector,
- $\mu$  is the Mars gravitational constant ( $\mu = 42828 \text{ km}^3/\text{s}^2$ ),
- $\bar{I}$  is the MEX inertia tensor.

Since the S/C Z-axis is nadir -pointing during the observation phase and the MEX inertia tensor in body axes is assumed as diagonal, there is nil gravity gradient torque during this period according to the model used. Therefore only the communication period needs to be considered (transition manoeuvres are ignored).

The angular momentum loading will be given then by the integral over the gravity gradient torque in inertial

$$\Delta \overline{H}_{gg}^{J2000} = \int \vec{T}_{gg}^{J2000}(t) dt \quad (50)$$

axes along the Earth-pointing period. Since the attitude during this phase is quasi-inertial (section 5.2) the ma-

---

<sup>1</sup>. For the cases with  $\|\vec{\Omega} \times \vec{r}\| \ll \|\vec{v}\|$  the following approach can be done: For these cases the X-axis is perpendicular to the orbital plane defined by the position and velocity wrt Mars. Within this approach the X-axis does not vary practically during one orbit and the second integral of eq.38 may be expressed as:

$$\hat{e}_x = \pm \frac{\vec{r} \times (\vec{v} - \vec{\Omega} \times \vec{r})}{|\vec{r} \times (\vec{v} - \vec{\Omega} \times \vec{r})|} \approx \frac{\vec{r} \times \vec{v}}{|\vec{r} \times \vec{v}|} \quad (1)$$

where the interval of observation is evaluated from Kepler's equation assuming an observation arc symmetric wrt the pericentre:

$$B = \int \hat{e}_x \cdot \hat{s} dt \approx \hat{s} \cdot \int \hat{e}_x dt \approx \hat{s} \cdot \hat{e}_x \Delta t_{obs} \quad (2)$$

where the interval of observation is evaluated from Kepler's equation assuming an observation arc symmetric wrt the pericentre:

$$\Delta t_{obs} = 2 \sqrt{\frac{a^3}{\mu}} (E_f - e \sin E_f) \quad (3)$$

The optimal value of the angle of orientation of the SA for the cases with  $\|\vec{\Omega} \times \vec{r}\| \ll \|\vec{v}\|$  may be approached by an analytical expression easy to handle with:

$$\Theta_{max} = \arctan\left(\frac{B}{A}\right) = \arctan\left(\frac{\hat{s} \cdot \hat{e}_x (E_f - e \sin E_f)}{-\hat{s} \cdot \hat{u}_P (\sin E_f - e E_f)}\right) \quad (4)$$

trix of transformation from the reference inertial axes (J2000) to the body-axes (quasi-inertial during the communication period) is nearly independent of time for the temporal range of interest. It means that in this particular case the integral may be effected in the S\C (quasi-inertial) axes:

$$\Delta \overrightarrow{H}_{gg}^{S\backslash C} = 3\mu \int \frac{\overrightarrow{u}(t) \times \bar{\bar{I}} \overrightarrow{u}(t)}{[r(t)]^3} dt \quad (51)$$

Since the inertia tensor in S/C axes is taken as diagonal the cross-product may be rewritten as:

$$\dot{\vec{u}} \times \bar{\bar{I}} \dot{\vec{u}} = \begin{bmatrix} (I_z - I_y)u_z u_y \\ (I_x - I_z)u_x u_z \\ (I_y - I_x)u_x u_y \end{bmatrix} \quad (52)$$

The variation of the nadir-pointing unit vector is easily shown in terms of the true anomaly as indicated in the figure 25:

$$\dot{\vec{u}} = -\cos v \dot{\vec{u}}_P - \sin v \dot{\vec{u}}_Q \quad (53)$$

where  $\dot{\vec{u}}_P$  and  $\dot{\vec{u}}_Q$  are the reference unit vectors, also assumed as constant for our purposes.

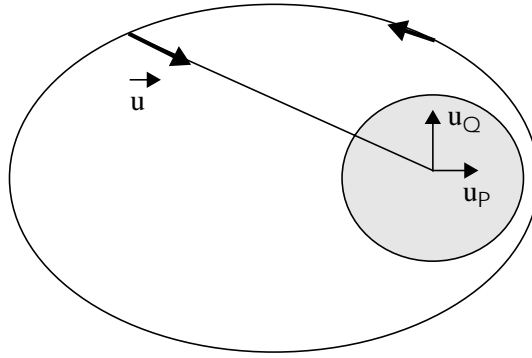


**Fig. 25. Nadir-pointing sketch**

Admitting that these reference vectors may be expressed in S/C axes and inserting eq.53 in eq. 52 yields

$$\dot{\vec{u}} \times \bar{\bar{I}} \dot{\vec{u}} = (\cos v)^2 \dot{\vec{b}} + (\sin v)^2 \dot{\vec{c}} + \sin v \cos v \dot{\vec{d}} \quad (54)$$

where the next constant vectors have been used:

$$\dot{\vec{b}} = \dot{\vec{u}}_P \times \bar{\bar{I}} \dot{\vec{u}}_P = \begin{bmatrix} (I_z - I_y)u_{Pz}u_{Py} \\ (I_x - I_z)u_{Px}u_{Pz} \\ (I_y - I_x)u_{Px}u_{Py} \end{bmatrix} \quad (55)$$

$$\dot{\vec{c}} = \dot{\vec{u}}_Q \times \bar{\bar{I}} \dot{\vec{u}}_Q = \begin{bmatrix} (I_z - I_y)u_{Qz}u_{Qy} \\ (I_x - I_z)u_{Qx}u_{Qz} \\ (I_y - I_x)u_{Qx}u_{Qy} \end{bmatrix} \quad (56)$$

$$\vec{d} = \vec{u}_P \times \vec{\bar{I}} \vec{u}_Q + \vec{u}_Q \times \vec{\bar{I}} \vec{u}_P = \begin{bmatrix} (I_z - I_y)(u_{Pz}u_{Qy} + u_{Qz}u_{Py}) \\ (I_x - I_z)(u_{Px}u_{Qz} + u_{Qx}u_{Pz}) \\ (I_y - I_x)(u_{Px}u_{Qy} + u_{Qx}u_{Py}) \end{bmatrix} \quad (57)$$

The angular momentum may be then expressed as:

$$\Delta \overrightarrow{H}_{gg}^{S \setminus C} = 3\mu \left( \vec{b} \int \frac{(\cos v)^2}{r^3} dt + \vec{c} \int \frac{(\sin v)^2}{r^3} dt + \vec{d} \int \frac{\sin v \cos v}{r^3} dt \right) \quad (58)$$

To evaluate these integrals let us rewrite them in terms of the true anomaly. The second Kepler's law assures the conservation of the area rate  $\dot{A}$  and thus:

$$\frac{1}{2} r^2 \frac{dv}{dt} = \dot{A} \Rightarrow \frac{dt}{r^2} = \frac{1}{2\dot{A}} dv \quad (59)$$

where for elliptic orbit the area rate is given by:

$$\dot{A} = \frac{\sqrt{\mu a(1-e^2)}}{2} \quad (60)$$

On the other hand from the polar equation of the elliptic orbit the inverse of the distance is also function of the true anomaly:

$$\frac{1}{r} = \frac{1 + e \cos v}{a(1 - e^2)} \quad (61)$$

Fortunately inserting equations 59 and 61 in eq 58 yields:

$$\Delta \overrightarrow{H}_{gg}^{S \setminus C} = 3 \sqrt{\frac{\mu}{\langle a(1 - e^2) \rangle}} (\vec{b}B + \vec{c}C + \vec{d}D) \quad (62)$$

where:

$$B = \int \left( (\cos v)^2 + e(\cos v)^3 \right) dv \quad (63)$$

$$C = \int \left( (\sin v)^2 + e \cos v (\sin v)^2 \right) dv \quad (64)$$

$$D = \int (\sin v \cos v + e \sin v (\cos v)^2) dv \quad (65)$$

These integrals admit direct analytical integration. For instance, if the angular momentum per orbit is to be calculated, integration must be done along the communication arc. Because of the symmetry of the arc wrt the pericentre line the integral D vanished and B and C result in:

$$B = \pi - v_c - \sin v_c \cos v_c - 2e \left( \sin v_c - \frac{(\sin v_c)^3}{3} \right) \quad (66)$$

$$C = \pi - v_c + \sin v_c \cos v_c - 2e \frac{(\sin v_c)^3}{3} \quad (67)$$

where  $v_c$  is the true anomaly at the beginning of the communication phase. It can be related with the eccentric anomaly through:

$$\tan \frac{v_c}{2} = \sqrt{\frac{1+e}{1-e}} \tan \frac{E_c}{2} \quad (68)$$

and accordingly with the maximum altitude of the observation phase  $h_{obs}$  as in eq. 47

$$E_c = \arccos \left( \frac{1 - \frac{h_{obs} + R_{Mars}}{a}}{e} \right) \quad (69)$$

The computation of the gravity gradient momentum loading per orbit by means of this analytical approach requires much less CPU-time than the direct integration of the torque. Besides it is coherent with the accuracy of the data and models used.

### 11. APPENDIX III: ANGULAR RATES DURING THE OPERATIONAL PHASE

For a complete description of the attitude evolution during the phases of interest the S/C rates are also calculated. In a general case let  $\vec{u}$  be a unit vector attached to the spacecraft. Its derivative is given by eq.70: ‘

$$\dot{\vec{u}} = \vec{\omega} \times \vec{u} \quad (70)$$

where  $\vec{\omega}$  is the S/C angular velocity.

Multiplying this expression by another unit vector of the spacecraft  $\vec{u}_\perp$  perpendicular to  $\vec{u}$  yields:

$$\vec{u}_\perp \cdot \dot{\vec{u}} = \vec{u}_\perp \cdot (\vec{\omega} \times \vec{u}) = \vec{\omega} \cdot (\vec{u} \times \vec{u}_\perp) \quad (71)$$

Derivating the relation of orthogonality between the S/C vectors,

$$\vec{u}_\perp \cdot \vec{u} = 0 \quad (72)$$

leads to:

$$\vec{u}_\perp \cdot \dot{\vec{u}} = -\dot{\vec{u}}_\perp \cdot \vec{u} \quad (73)$$

Making application to the S/C frame unit vectors, equations 71 and 73 allow formulating the S/C rates in a compact form:

$$\omega_x = -\dot{\vec{e}}_z \cdot \vec{e}_y = \dot{\vec{e}}_y \cdot \vec{e}_z \quad (74)$$

$$\omega_y = \dot{\vec{e}}_z \cdot \vec{e}_x = -\dot{\vec{e}}_x \cdot \vec{e}_z \quad (75)$$

$$\omega_z = -\dot{\vec{e}}_y \cdot \vec{e}_x = \dot{\vec{e}}_x \cdot \vec{e}_y \quad (76)$$

### 11.1. Nadir-pointing attitude rates

Once the nominal observation attitude is defined, the rates can be calculated according to eqs. 74, 75 and 76.

The derivative of the Z-axis (nadir-pointing) remains in the orbital plane.

$$\dot{\vec{e}}_z = -\vec{v} \frac{1}{|\vec{r}|} - \vec{r} \frac{d\left(\frac{1}{|\vec{r}|}\right)}{dt} \quad (77)$$

On the other hand, as shown in expression 78:

$$\dot{\vec{e}}_z = \vec{\omega} \times \vec{e}_z \Rightarrow \vec{e}_z \times \dot{\vec{e}}_z = \vec{e}_z \times (\vec{\omega} \times \vec{e}_z) = \vec{\omega} - (\vec{\omega} \cdot \vec{e}_z) \vec{e}_z \quad (78)$$

the total angular velocity can be rewritten as:

$$\vec{\omega} = \vec{e}_z \times \dot{\vec{e}}_z + \omega_z \vec{e}_z \quad (79)$$

where the cross-product corresponds to:

$$\vec{e}_z \times \dot{\vec{e}}_z = \frac{\vec{r}}{|\vec{r}|} \times \left( \vec{v} \frac{1}{|\vec{r}|} + \vec{r} \frac{d\left(\frac{1}{|\vec{r}|}\right)}{dt} \right) = \frac{\vec{r} \times \vec{v}}{\vec{r} \cdot \vec{r}} \quad (80)$$

Inserting it in eq.79 yields:

$$\vec{\omega} = \frac{\vec{r} \times \vec{v}}{\vec{r} \cdot \vec{r}} + \omega_z \vec{e}_z \quad (81)$$

Equation 81 shows that the angular velocity can be separated in two terms. The first term is orthogonal to the orbital plane and corresponds to the minimum angular rotation necessary to point towards a target (Mars in this case). It leads to the rates on X-axis and Y-axis. The second term represents an additional rotation around the direction to the target.

Derivating eq.2 and inserting it into eq.76 yields the angular rate on Z-axis:

$$\omega_z = \dot{\vec{e}}_x \cdot \vec{e}_y = \pm \frac{\left( \vec{r} \times \frac{d\vec{v}}{dt} \right) \cdot \vec{e}_y + (\vec{\Omega} \cdot \vec{r})(\vec{v} \cdot \vec{e}_y) - 2(\vec{v} \cdot \vec{r})(\vec{\Omega} \cdot \vec{e}_y)}{|\vec{r} \times (\vec{v} - \vec{\Omega} \times \vec{r})|} \quad (82)$$

where the cross product of the position and the acceleration may be neglected since the force field is mainly central.

The resulting rates for the second observation period after MOI are shown in figures 26 and 27:

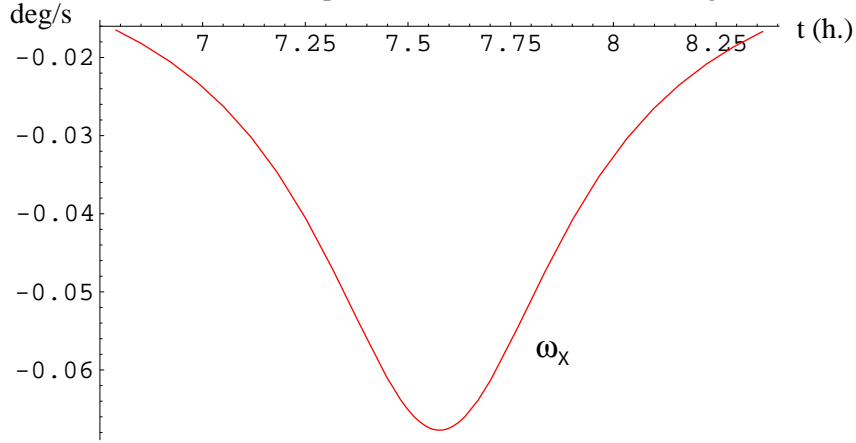


**Fig. 26. Angular rate on the X-axis during observation phase**

Since the X-axis is almost perpendicular to the orbital plane defined by the MEX position and velocity wrt Mars, the angular rate on X-axis is much higher than the rates on the other axes.

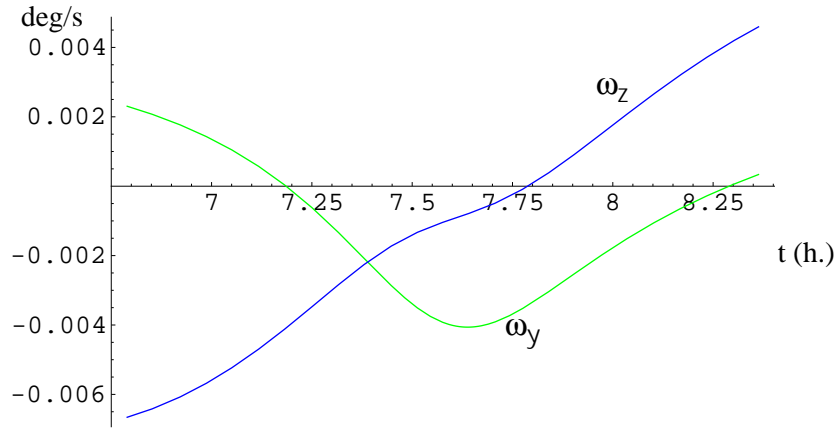


**Fig. 27. Angular rates on the Y-axis and Z-axis during observation phase**

### 11.2. Earth-pointing attitude rates

The defined attitude of the communication mode is quasi-inertial since the relative positions of Earth and sun wrt MEX do not change significantly throughout an orbit.

Therefore the S/C angular rates may be neglected at first approach. In any case the formal expression of these rates is written as

$$\omega_z = \frac{\dot{\vec{r}}_E \cdot \vec{e}_y}{|\dot{\vec{r}}_E|} \quad (83)$$

$$\omega_y = -\frac{\dot{\vec{r}}_E \cdot \vec{e}_z}{|\dot{\vec{r}}_E|} \quad (84)$$

$$\omega_x = -\dot{\vec{e}}_z \cdot \vec{e}_y = \dot{\vec{e}}_y \cdot \vec{e}_z \quad (85)$$

## **12. ACRONYMS AND ABBREVIATIONS**

AU	Astronomical Unit
CoM	Center of Mass
CoP	Center of Pressure
d	days
h	hours
HGA	High Gain Antenna
max.	maximum
MEX	Mars EXpress
min.	minimum
MOI	Mars Orbit Insertion
RCS	Reaction Control System
RCT	Reaction Control Thruster
RW	Reaction Wheels
SA	Solar Array
SADM	Solar Array Drive Mechanism
S/C	Spacecraft
TBC	To Be Confirmed
TBD	To Be Defined
TN	Technical Note
WOL	Wheels Off-loading
wrt	with respect to

## **13. ACKNOWLEDGEMENTS**

The work described in this paper was supported by GMV S.A., under a contract with ESOC. Special thanks to Mr. Companys and Mr. Fertig for the supervision from ESOC/Flight Dynamics-Interplanetary Missions. A lot of good suggestions and the idea to combine rotation manoeuvres come from Mr. Companys. Further thanks to Mr. Hechler and Mr Yáñez for the inputs from Mission Analysis.

## **14. REFERENCES**

- [1] Hechler M., Yáñez, A.: "MARS EXPRESS Mission Analysis: S/C Power, Earth and Lander Communications", MAS Working Paper No.421,Draft,(September 1999).
- [2] Hechler M.: "MARS EXPRESS Reference Orbit " MAS (March 1999)
- [3] Hechler M.: " MARS EXPRESS Mission Assumptions Document" F1-MAD-MEX-001, Issue 1 (May 98)
- [4] Faye,F. (MMT MEx Team):"Mars Express Spacecraft Design Report", MEX-MMT-RP-0216, (May 1999)

- [5] Borde,J.: "Mars Express Mission Plan". MEX-MMT-RP-0221 (May 1999)
- [6] Lebranchu,C.: "S/C Characteristics for Cruise", MEX-MMT-FX-352-99 (October 1999)
- [7] Wertz,J.R.: "Spacecraft Attitude Determination and Control", Reidel Publishing Company (1984).
- [8] De Pasquale, E.: " Momentum Loading due to Disturbance Torques during Approach to Mars" RO-ESC-TN-5504 , Draft 1, (November 1998)
- [9] Roche,Y.: "Solar forces and torques on the solar arrays" RO-DSS-TN-1009 (June1997)
- [10] Bouffard, F.: "Thruster Modulator and Selection Functions. Definition and Justification" MEX.MMT.TN.0298 (June,1999)
- [11] Ecale, E.: "Reaction wheels Management Function. Definition and Justification" MEX.MMT.TN.0302 (June,1999)
- [12] Ecale, E.: "Reaction wheels Off-loading Function. Definition and Justification" MEX.MMT.TN.0298 (June,1999)
- [13] Elices, T.: "Introducción a la Dinámica Espacial", Instituto Nacional de Técnica Aeroespacial (1991).